electronics

MDPI

Article

Phase Diffusion in Low-E_J Josephson Junctions at Milli-Kelvin Temperatures

Wen-Sen Lu, Konstantin Kalashnikov, Plamen Kamenov, Thomas J. DiNapoli and Michael E. Gershenson *

Department of Physics and Astronomy, Rutgers University, Piscataway, NJ 08854, USA
* Correspondence: gersh@physics.rutgers.edu

Abstract: Josephson junctions (JJs) with Josephson energy $E_J \lesssim 1$ K are widely employed as non-linear elements in superconducting circuits for quantum computing operating at milli-Kelvin temperatures. In the qubits with small charging energy E_C ($E_J/E_C \gg 1$), such as the transmon, the incoherent phase slips (IPS) might become the dominant source of dissipation with decreasing E_J. In this work, a systematic study of the IPS in low-E_J JJs at milli-Kelvin temperatures is reported. Strong suppression of the critical (switching) current and a very rapid growth of the zero-bias resistance due to the IPS are observed with decreasing E_J below 1 K. With further improvement of coherence of superconducting qubits, the observed IPS-induced dissipation might limit the performance of qubits based on low-E_J junctions. These results point the way to future improvements of such qubits.

Keywords: superconducting; Josephson junction; phase slip; critical current; Josephson energy; quantum; quantum circuit; qubits

1. Introduction

Josephson junctions (JJs) with the Josephson energy 0.1 K$< E_J <$ 1 K have been recently employed as non-linear elements of superconducting qubits (see, e.g., [1–4]). Though E_J of these junctions remains much greater than the physical temperature of qubits ($\sim$20 $\div$ 50 mK), a non-zero rate of thermally-activated phase slips in these junctions might soon limit the coherence of superconducting qubits. Indeed, with the qubit coherence time exceeding 1 ms [5], even rare dissipative events might become significant. Thus, the study of incoherent phase slips, induced by either equilibrium (thermal) or non-equilibrium noise, might help better understand the limitations of the low-E_J JJs as elements of quantum circuits operating at mK temperatures.

In the past, phase slips in JJs [6] and associated phase diffusion [7–10] attracted a great deal of experimental and theoretical attention. This effort was mainly aimed at better understanding of a crossover from the classical Josephson behavior (well-defined phase difference, strong quantum fluctuations of charge) to the Coulomb-blockade regime (localized charges, strong quantum fluctuations of phase) (see, e.g., [11–14] and references therein). The crossover is observed in ultra-small JJs with the Josephson energy E_J of the same order of magnitude as the Coulomb energy $E_C = (2e)^2/(2C_J)$ (C_J is the effective JJ capacitance) provided the junctions are included in a circuit with the impedance Z greatly exceeding the quantum resistance $R_Q = h/(2e)^2 \approx 6.5k\Omega$. The rate of the coherent phase slip processes (the so-called quantum phase slips, or QPS) exponentially increases with decreasing the ratio E_J/E_C [15].

The qubit dephasing by QPS [16] has been considered for the charge-sensitive transmon qubits [17] and heavy fluxonium qubits [1,18,19]. However, energy relaxation due to the incoherent phase slips in the ubiquitous elements of the multi-qubit circuits, the charge-insensitive transmons, has never been addressed. To fill this gap, in the current paper the dissipative processes in the low-E_J Josephson junctions are systematically studied in the regime $E_J \gtrsim T \gg E_C$, which is relevant for operation of superconducting qubits

check for updates

Citation: Lu, W.-S.; Kalashnikov, K.; Kamenov, P.; DiNapoli, T.J.; Gershenson, M.E. Phase Diffusion in Low-E_J Josephson Junctions at Milli-Kelvin Temperatures. *Electronics* **2023**, *12*, 416. https://doi.org/10.3390/electronics12020416

Academic Editor: Michael I. Faley

Received: 7 December 2022
Revised: 9 January 2023
Accepted: 10 January 2023
Published: 13 January 2023

shunted with a large external capacitance [13–15]. In this regime, quantum fluctuations of charge are strongly enhanced and the QPS are suppressed. To explore the dynamics of low-E_J junctions at mK temperatures, we designed JJs with E_J = 0.1–1 K and $E_C < 10$ mK, and studied the IPS in these JJs with low-frequency transport measurements. The JJs in this work have been implemented as SQUIDs to allow in-situ tuning of E_J by the magnetic field.

The paper is organized as follows. In Section 2, the known facts about the phase diffusion induced by incoherent phase slips in underdamped JJs are briefly reviewed. The sample design and experimental techniques are discussed in Section 3. The measurements of current-voltage characteristics (IVC) of low-E_J devices are presented in Section 4. In Section 5, our results and the data reported by other groups are discussed with the focus on implications of the dissipation induced by incoherent phase slips for the operation of qubits that employ low-E_J Josephson junctions. The conclusions are presented in Section 6.

2. Phase Diffusion in Underdamped Junctions

At $T = 0$, the critical current I_C^{AB} of a "classical" JJ ($E_J \gg E_C$) is provided by the Ambegaokar–Baratoff relation [6]

$$I_C^{AB}(T=0) = \frac{2e}{\hbar} E_J = \frac{\pi \Delta(0)}{2eR_N}, \quad (1)$$

where Δ is the superconducting energy gap and R_N is the normal-state resistance of a JJ. This relation has been derived by neglecting phase fluctuations. In the absence of non-equilibrium noise and charging effects, the voltage drop across a JJ is expected to be zero at $I < I_C^{AB}(T=0)$. The quantum phase fluctuations, which become strong at $E_J \lesssim E_C$, result in the so-called coherent quantum phase slips (CPS) in one-dimensional JJ chains (see [20–22] and references therein). The junction capacitance C plays the role of the effective mass of a fictitious particle that tunnels between the minima of the "washboard" potential $U(\varphi) = -E_J \cos\varphi - \frac{\hbar I}{2e}\varphi$ [6]. Reduction of C and, thus, increase of E_C, facilitates tunneling and promotes CPS. The CPS shift the system energy levels and renormalize the effective Josephson coupling $E_J^* \sim E_J^2/E_C$. The CPS also result in energy dissipation in one-dimensional superconducting wires [23,24] as well as in the external circuits connected to the Josephson junctions.

In the regime $E_J \gg E_C$, on the other hand, the incoherent classical phase slips (IPS) induced by either non-zero temperature or non-equilibrium noise are expected to dominate. The IPS correspond to the over-the-barrier activation in the washboard potential [6]. In thermal equilibrium, the IPS rate depends exponentially on the temperature: $\nu_{IPS} \propto \omega_p e^{-\Delta U/k_B T}$ [6]. Here, $\omega_p = \frac{1}{\hbar}\sqrt{2E_J E_C}$ is the plasma frequency which plays the role of the attempt rate, ΔU is the height of the potential barrier, which is close to $2E_J$ at currents $I \ll I_C^{AB}$.

The IPS process is analogous to a single flux quantum Φ_0 crossing a JJ (the process is dual to the transfer of a single Cooper pair through the JJ [25]). Each phase slip generates a voltage drop $V(t)$ across the JJ, such that $\int V(t)dt = \Phi_0$ and, in the presence of a current I, releases an energy $I\Phi_0$. Thus, the zero-voltage state can be destroyed by the energy dissipation due to the time-dependent phase fluctuations. At zero tilt of the "washboard" potential $U(\varphi)$, the phase slips with different signs of the phase change occur with the same probability and, as a result, the average voltage across the junction is zero. However, when the junction is biased with a non-zero current I, the tilt of the washboard potential breaks the symmetry and a non-zero average voltage proportional to the phase slip rate is generated across the junction.

The dynamics of JJs depends on all sources of dissipation, such as IPS, thermally excited quasiparticles, etc. The low-dissipative (underdamped) regime, observed at $T \ll \Delta$ and in a high-impedance environment, is relevant to the operation of superconducting qubits. Typically, dissipation is highly frequency-dependent: it is strongly suppressed at low frequencies $\omega \ll \omega_p$ and, potentially, significantly enhanced at frequencies approaching ω_p. This frequency-dependent dissipation leads to the phenomenon of underdamped phase diffusion [7,8,26]. Characteristic signatures of this regime are the absence of the zero-

voltage superconducting state and the existence of a low-voltage ($V \ll \frac{2\Delta}{e}$) IVC branch, which extends up to $I_{SW} \ll I_C^{AB}$. The IVC is hysteric at currents $I < I_{SW}$: the low-V branch observed with increasing the current from 0 to I_{SW} coexists with a high-voltage ($V \geq \frac{2\Delta}{e}$) branch observed with decreasing the current from $I > I_{SW}$ to zero. At high voltages $V > \frac{2\Delta}{e}$, the main dissipation mechanism is the Cooper pair breaking and generation of non-equilibrium quasiparticles. In the low-voltage state $V < \frac{2\Delta}{e}$, the energy gained by a system in the process of the over-the-barrier activation is dissipated mostly due to the Josephson radiation [27].

The theory of the DC transport in underdamped Josephson junctions in the regime $E_C \ll T \leq E_J < \Delta$ in presence of a stochastic noise has been developed by Ivanchenko and Zilberman [28] (the IZ theory, see Appendix C). The IZ theory predicts that $I_{SW} \propto E_J^2$ at small E_J [29], in contrast to the dependence $I_C^{AB} \propto E_J$ for the regime $E_C, T \ll E_J$ (Equation (1)).

More recent analysis of the effect of non-zero temperature in the underdamped junctions was provided by Kivioja et al. [30]. By considering the quality factor at the plasma frequency, $Q(\omega_p)$, and the energy dissipated between adjacent potential maxima $\Delta E_D \approx 8E_J/Q(\omega_p)$, Kivioja et al. showed that the maximum possible power dissipated due to phase diffusion before switching to a state with $V \approx 2\Delta/e$ can be expressed as

$$\frac{2\pi V}{\Phi_0} \times \frac{\Delta E_D}{2\pi} = V \times I_{SW}, \tag{2}$$

where $I_{SW} = 4I_C/\pi Q$ is the maximum possible current carried by underdamped junctions in the phase diffusion (UPD) regime. At $I < I_{SW}$, there is a non-zero probability for a fictitious particle to be retrapped after escape from a local minimum of the potential $U(\varphi)$. As a result, instead of a run-away state with $V = 2\Delta/e$, the IVC demonstrates a non-zero slope at $I < I_{SW}$ due to the phase diffusion. The value of R_0, therefore, provides valuable information regarding the nature of damping in the junction circuits.

3. Experimental Techniques

All the samples studied in this work have been implemented as SQUIDs, in order to be able to in-situ tune E_J by changing the magnetic flux Φ in the SQUID loop [6]:

$$E_J = 2E_{J0} \cos\left(\pi \frac{\Phi}{\Phi_0}\right), \tag{3}$$

Figure 1 schematically shows the design of a chain of SQUIDs formed by small (0.2×0.2 μm^2) JJs. The area of the SQUID loop, A_{SQUID}, varied between 6 μm^2 and 50 μm^2. The chains of SQUIDs had additional contact pads (shown in yellow in Figure 1) to provide access to individual SQUIDs or pairs of SQUIDs within a chain.

In order to reduce the rate of quantum phase slips $\nu_{QPS} \propto \exp(-\sqrt{\frac{2E_J}{E_C}})$ [6], either the low-transparency JJs junctions with a relatively large in-plane area A_{JJ} (> 1μm^2), or smaller junctions shunted with external capacitors (the design details are provided in Appendix A) have been used. In both cases, the charging energy E_C was reduced below ≈10 mK, and this allowed us to maintain a large ratio E_J/E_C for all studied JJs.

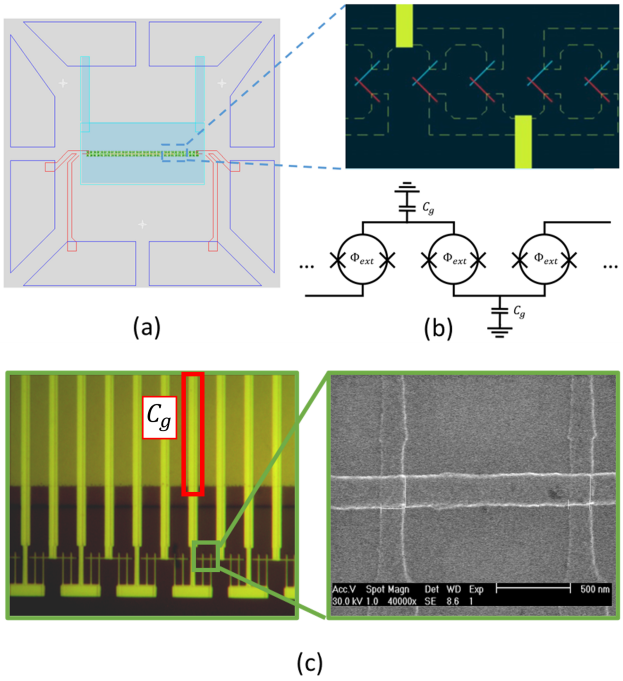

Figure 1. (**a**) Schematics of a chain of SQUIDs made of Josephson junctions with a relatively large area (i.e., large C_J) and a low transparency of the tunneling barrier (i.e., small E_J). The common ground electrode made of a sputtered Pt film is shown in pale blue. A few *nm* thick AlO_X oxide covers this electrode and serves as a pinhole-free dielectric that isolates the ground from the SQUIDs. The typical value of the capacitance that shunts a single SQUID, C_g, is 0.5 nF for 50 μm^2 pad area. This C_g corresponds to a charging energy per SQUID $E_C = \frac{(2e)^2}{2C_g} = 8$ mK. (**b**) The circuit diagram of a chain of SQUIDs. (**c**) An alternative design of a chain of SQUIDs shunted by external capacitors to the ground. The vertical 5 μm-wide pads are the ground electrodes for the capacitors, a few *nm* thick AlO_X serves as a dielectric between the electrodes.

The amplitude of variations of E_J with the external magnetic field depends on scattering of parameters of individual JJs that form a nominally symmetric SQUID. This scattering did not exceed 10% for the JJs with the normal-state resistance $R_N \approx 1$ kΩ and $A_{JJ} = 0.02$ μm^2. However, fabrication of the low-transparency JJs with $R_N \approx 100$ kΩ and $A_{JJ} = 4$ μm^2 (the nominal critical current density $I_C^{AB}/A_{JJ} \approx 5 \times 10^{-4} A/\text{cm}^2$), which required very long oxidation times and high partial pressure of O_2, resulted in a larger (≈30%) scattering of the R_N values (Appendix A). This scattering was one of the reasons for different dependence $I_{SW}(B)$ observed for the nominally identical SQUID chains (see below). The parameters of representative samples are listed in Table 1 (the total number of tested samples exceeded 50 [31]).

Table 1. Parameters of single Josephson junctions in SQUID chains. R_N and A_{JJ} are the normal-state resistance and the junction area, respectively. The Josephson energy $E_J = \pi\hbar\Delta/((2e)^2 R_N)$ has been calculated using R_N and $T_C = 1.3$ K . The charging energy E_C, where C is the shunting capacitance, did not exceed 10 mK for all samples. The critical current I_C^{AB} was calculated using Equation (1).

Sample	R_N (kΩ)	E_J (K)	A_{JJ} (μm^2)	I_C^{AB}	I_{SW} (nA)
1	2.4	2.9	1.9	130	48
2	2.9	2.4	3.74	107	68
3	9.4	0.76	0.04	33	9
4	15.8	0.45	0.04	20	0.3
5	16.6	0.43	0.04	19	0.1
6	175	0.04	0.04	1.8	0.003

4. Current-Voltage Characteristics of Low-E_J Junctions

The results below focus on data obtained at $T < 200$ mK—in this temperature range one can neglect transport of the thermally-excited quasiparticles in Al-based superconducting circuits. Typical IVC measured at $T_{base} = 25$ mK for the samples with $E_J \approx 1$ K and $E_J \ll 1$ K are shown in Figure 2. Several characteristic features of the IVC are addressed below.

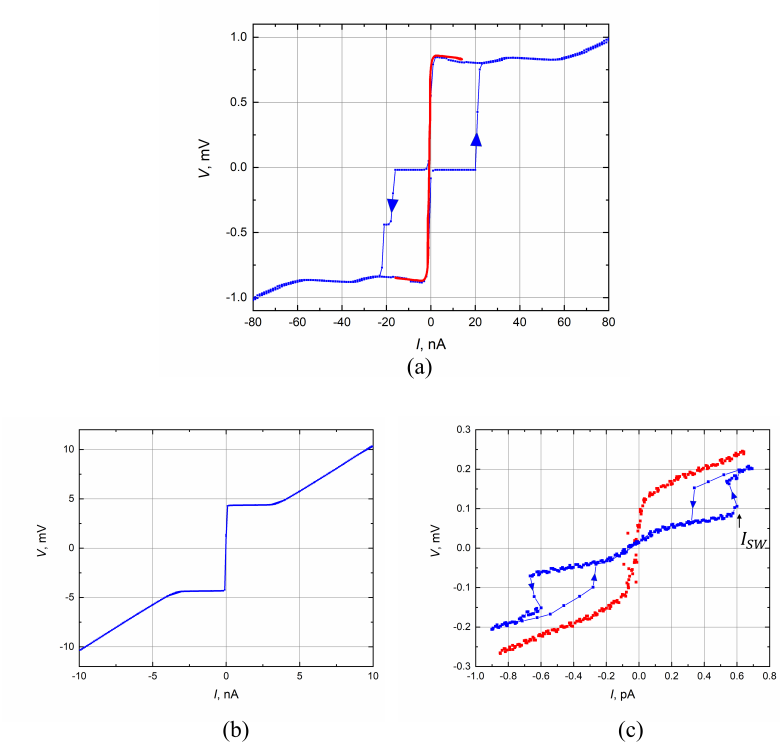

Figure 2. (**a**) Current-voltage characteristics of two connected-in-series SQUIDs at $\Phi = 0$ (blue curve) and $\Phi = 0.5\Phi_0$ (red curve) at $T \approx 30$ mK. Each SQUID is formed by two nominally identical JJs with $E_J = 0.76$ K (sample 3 in Table 1), thus the SQUID Josephson energy is $1.52K$. Even for this circuit with relatively high E_J, the measured switching current per junction, $I_{SW} = 9$ nA, is significantly lower than $I_C^{AB} = 33$ nA. (**b**) The IVC of a chain of 20 SQUIDs with $E_J = 80$ mK (for single-JJ parameters, see sample 6 in Table 1). (**c**) The enlargement of the region of small currents/voltages in panel (**b**). Note that the resistance is non-zero for all biasing currents. The switching current (its value for a given sample, 0.6 pA, is indicated by an arrow) corresponds to a rapid increase of the voltage across the chain. This switching current is almost four orders of magnitude smaller than the I_C^{AB} value for this sample (see Table 1). The zero-bias resistance ($R_0 \approx 500$ MΩ per junction) was determined as the slope of the IVC at $I \ll I_{SW}$.

4.1. The Switching Current I_{SW} and the Zero-Bias Resistance R_0

Figure 2 shows how the switching current I_{SW} and the zero-bias resistance R_0 measured at small DC voltages $V \ll 2\Delta/e$ and currents $I \ll I_{SW}$ are determined. Note that the zero-bias resistance per junction is twice as large as the zero-bias resistance of a SQUID. For the JJs with $E_J = 0.76$ K (Figure 2a) a non-zero R_0 could not be detected within the accuracy of measurements conducted in this work ($\approx 10^2 \sim 10^3\Omega$, depending on the magnitude of I_{SW}). This is the behavior expected in the "classical" regime $E_J \gg T, E_C$. At currents $I > I_{SW}$, the voltage across the chain approaches the value $N \times 2\Delta/e$, where N is the number of SQUIDs in the chain and $2\Delta \approx e \times 0.4$ mV is the sum of superconducting energy gaps in the electrodes that form a junction. For the chains with $E_J \ll 1$ K, the switching current is several orders of magnitude smaller than the Ambegaokar–Baratoff critical current (Figure 2c). With the magnetic field B approaching the value $\Phi_0/(2A_{SQUID})$,

the switching current vanishes and R_0 increases by orders of magnitude (red curves in Figure 2a,c). The IVC at $\Phi = \Phi_0/2$ resemble that observed in the Coulomb-blockade regime. Note that for most of the studied samples in this regime E_C is close to the base temperature, so the Coulomb blockade is partially suppressed by thermal effects. The resistance $R_0(\Phi = \Phi_0/2)$ for the samples with $E_J \ll 1$ K is limited by the input resistance of the preamplifier (a few $G\Omega$).

The evolution of the IVC measured at different temperatures for $\Phi = \Phi_0/2$ is shown in Figure 3a. The $R_0(T)$ drop observed with an increase of temperature at $T > 0.2$ K (Figure 3b) is due to an increasing concentration of thermally excited quasiparticles in *Al* electrodes: the JJ becomes "shunted" by the quasiparticle current. The dependence $R_0(T)$ at $T > 0.25$ K can be approximated by the Arrhenius dependence $R_0(\Phi = \Phi_0/2, T) \propto exp(\delta/k_BT)$ with $\delta \approx 2.1$ K. The activation energy δ is close to the superconducting energy gap $\Delta \approx 2.3$ K in Al electrodes with $T_C \approx 1.3$ K.

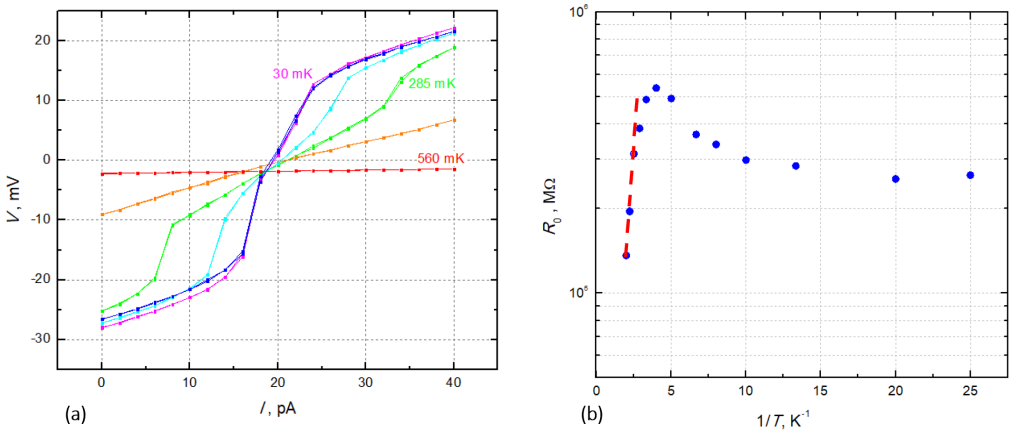

Figure 3. (**a**) Current-voltage characteristics of two connected in series SQUIDs measured at $\Phi = 0.5\Phi_0$ and different temperatures (from 30 mK to 560 mK, as shown in the panel). The SQUIDs are formed by JJs with $E_J = 0.76$K (sample 3 in Table 1). (**b**) The temperature dependence of the zero-bias resistance for this sample. The red dashed line corresponds to the dependence $R_0(\Phi = 0.5\Phi_0, T)$ = 4 kΩ × exp(δ/T) with $\delta = 2.1$ K.

4.2. The IVC Hysteresis

For all studied samples, strong hysteresis of the IVC is observed at $\Phi = n\Phi_0$ where n is integer. The hysteresis is a signature of the underdamped junctions with the McCumber parameter $\beta \gg 1$ [32]. Observation of the hysteresis is also an indication that the noise currents I_N in the measuring setup are significantly smaller than the switching current even for the samples with I_{SW} in the sub-pico-A range (in the opposite limit, $I_N > I_{SW}$, the hysteresis vanishes, see Appendix C and Ref. [33]).

4.3. The $I_{SW}(B)$ Dependences

Even in the "classical" regime $E_J \gg E_C, T$, several unexpected results are obtained. Firstly, the dependence of $I_{SW}(\Phi)$ for some samples significantly deviated from the dependence

$$I_{SW}(\Phi) = I_{SW}(\Phi = 0) \times \mid \cos(\pi \frac{\Phi}{\Phi_0}) \mid, \quad (4)$$

(see Figure 4c). These deviations can be at least partially explained by a relatively large scattering of parameters of individual JJs and non-uniformity of the local magnetic field in the SQUID loops due to the magnetic field focusing. Observation of a steeper drop of I_{SW} with $\Phi \to 0.5\Phi_0$ than that predicted by Equation (3) can be attributed to violation of the condition $E_J(\Phi) \gg E_C$ and crossover to the Coulomb blockade regime.

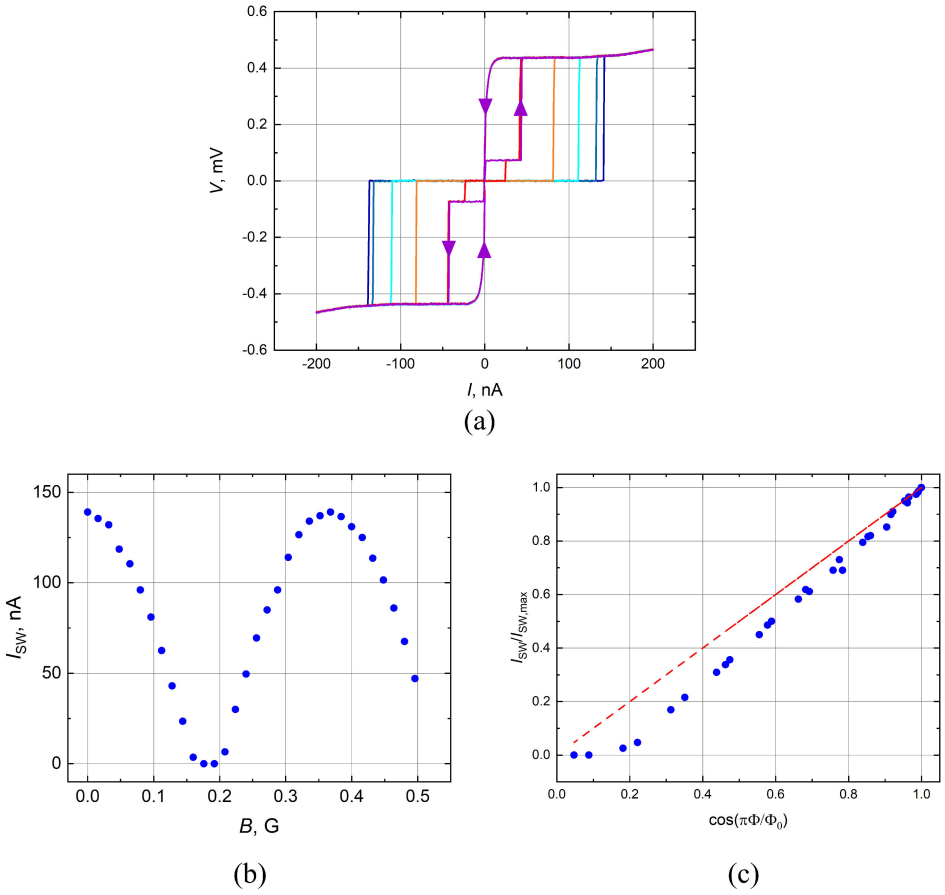

Figure 4. (**a**) Current-voltage characteristics of a single SQUID formed by JJs with $E_J = 2.4$ K (sample 2 in Table 1) measured at different values of $\Phi/\Phi_0 = 0, 0.08, 0.17, 0.25, 0.37, 0.5$. A sub-gap voltage plateau at $V \approx 75$ μV appears at $\Phi > 0.35\Phi_0$. For different samples the sub-gap voltage plateau was observed at V = 40–200 μV. (**b**) The dependence of I_{SW} on the magnetic field B. (**c**) The measured $I_{SW}(\Phi)/I_{SW}(\Phi = 0)$ as a function of $cos(\pi\Phi/\Phi_0)$. The dashed line corresponds to the dependence $I_{SW} \propto cos(\pi\Phi/\Phi_0)$.

Secondly, sub-gap ($V_{subgap} < 2\Delta/e$) voltage steps on the IVC are observed (Figure 4a), which significantly reduced the accuracy of extraction of I_{SW} and R_0 at the values of Φ close to $\Phi_0/2$. A possible reason for appearance of sub-gap steps might be the Fiske resonances due to the microwave resonant modes of the circuit [34]. Identifying the circuit elements that would be responsible for the corresponding resonance frequencies at $f_{res} = (75\ \mu eV)/h \approx 18$ GHz (this frequency corresponds to a wavelength ∼2.5 mm for the electromagnetic wave propagating along the interface between a silicon substrate and vacuum) requires further investigation.

5. Discussion

There are several potential sources of dissipation in Josephson circuits at $T \ll \Delta$, such as non-equilibrium quasiparticles or two-level systems in the circuit environment (see, e.g., [35] and references therein). However, we are unaware of a mechanism other than the IPS that would explain the observed strong dependence of dissipation on the ratio E_J/T. Below, we focus on the IPS as the dominant dissipation mechanism in this work.

5.1. The Switching Currents I_{SW}

The results of I_{SW} measurements for samples with different E_J are summarized in Figure 5. Here, the data for four samples are plotted at different values of external magnetic flux threading the SQUIDs loop. The effective E_J for these devices was calculated using

Equation (2). For comparison, in Figure 5 the I_{SW} data reported in literature for the JJs with large values of E_J/E_C are also plotted. Scattering of I_{SW} values at a given E_J can be attributed, at least partially, to different noise levels in different experimental setups, and to a relatively wide range of E_J/E_C values (see Table 2)—proliferation of QPS with decreasing E_J/E_C can strongly reduce I_{SW}. Despite the data scattering, the general trend is clear: with decreasing E_J, the switching current decreases significantly faster than the linear dependence $I_{SW}(E_J)$ predicted by the Ambegaokar–Baratoff relationship (Equation (1)). At $E_J = 0.1$ K, I_{SW} is already two orders of magnitude smaller than $I_C^{AB}(T = 0)$.

Qualitatively, the data are in agreement with theory of the DC transport in underdamped Josephson junctions with $E_C \ll E_J$ developed by Ivanchenko and Zilberman [28]. In the regime $E_C \ll T \leq E_J < \Delta$, dissipation in the JJ circuits is associated with IPS induced by either an equilibrium noise generated by thermal excitation or a non-equilibrium noise. According to the IZ theory, the equation for the phase φ across a classical Josephson junction ($E_C \ll E_J$) can be written as

$$\frac{2e}{\hbar}(I_b + I_n) = \frac{1}{R}\frac{\partial \varphi}{\partial t} + \frac{2e}{\hbar} I_C sin\varphi, \tag{5}$$

where I_b is the bias current, $\langle I_n(0) I_n(\tau)\rangle \geq \frac{2k_B T}{R}\delta(\tau)$ is the delta-correlated Johnson–Nyquist noise across the resistance R connected in parallel with the junction. The superconducting part of the current as a function of bias voltage V_B can be found by solving the corresponding Fokker–Planck equation (see Appendix D). With decreasing E_J, the theory predicts a ***quadratic*** drop of the maximum superconducting current that the junction can sustain (i.e., the switching current I_{SW}) [29]. This maximum value of the switching current is realized at a non-zero voltage V_n, which depends only on the voltage noise amplitude, so the zero-bias resistance in the IPS regime is expected to scale as E_J^{-2} .

The dependence $I_{SW}(E_J)$ predicted by the IZ theory in presence of additional Gaussian noise with amplitude of $V_{noise} = 24$ μV is plotted in Figure 5. This noise corresponds to the Johnson–Nyquist noise $\delta V_t = \sqrt{4k_B T R \Delta f}$ generated at $T = 50$ mK by two 100 kΩ resistors connected in series with the device (Figure A2 in Appendix B). These chip resistors, designed for microwave applications, had a very small imaginary part of their impedance. The bandwidth was estimated as $\Delta f \approx \omega_p/2\pi$, where $\omega_p/2\pi \approx 1$ GHz is the plasma frequency of the shunted JJs. Though the theory (the solid curve in Figure 5) is in qualitative agreement with the experimental data, most of the experimental I_{SW} values are an order-of-magnitude smaller than I_{SW} predicted by the IZ theory. A possible explanation for this discrepancy might be more complex phase dynamics in the devices with a very high IPS rate, outside of the limits of applicability of the IZ theory. Another possibility is the exponentially strong sensitivity of the IPS rate to the noise level in different setups and the physical temperature of samples, the parameters that are not easy to control in most experiments.

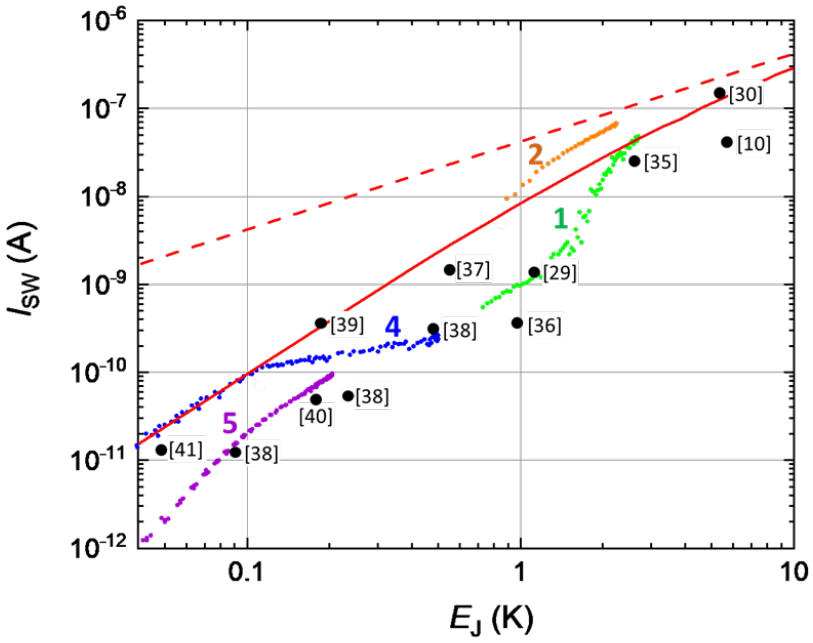

Figure 5. The switching current I_{SW} as a function of E_J measured in experiments conducted in this work (the color-coded symbols, the sample numbers correspond to that in Table 1) and by other experimental groups (black dots, the references are given in square brackets). All the data have been obtained at $T \approx 20$–50 mK for $Al/AlO_X/Al$ junctions. For the values of I_{SW} measured at $B \neq 0$ the Josephson energy $E_J(B)$ was calculated using Equation (2). The dashed red line corresponds to the Ambegaokar–Baratoff dependence $I_C^{AB}(E_J)$ (Equation (1)), the solid red curve—to the switching current predicted by the IZ theory in presence of additional V_{noise} = 24 μV generated by the biasing scheme (see Appendix D).

5.2. The Zero-Bias Resistance R_0

Figure 6 shows R_0 as a function of E_J measured in this work and by other groups for $Al/AlO_X/Al$ junctions. To simplify the Figure, the data in this work are plotted only for the sample with the lowest values of R_0 (sample 5); R_0 for other samples are approximately in line with the data from literature shown in Figure 6. The zero-bias resistance, being unmeasurably low at $E_J > 1$ K, rapidly increases at $E_J < 1$ K, and becomes much greater than the normal-state resistance R_N at $E_J \leq 0.1$ K. Instead of a well-defined "superconductor-to-insulator" transition at a certain value of E_J/E_C, a broad crossover between these two limiting regimes is observed. Note that different JJ samples (single junctions and arrays) demonstrate similar values of R_0, though their charging energies could vary over a wide range.

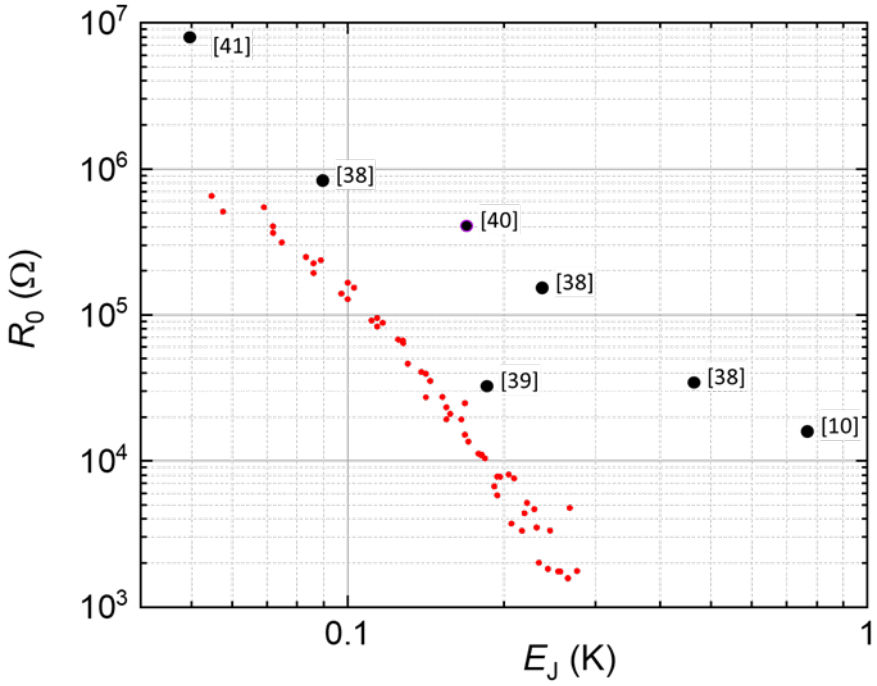

Figure 6. The zero-bias resistance R_0 as a function of E_J measured for a chain of SQUIDs made of JJs with $E_J = 0.43$ K (sample 5 in Table 1) (red dots). For comparison, the values of R_0 measured by other experimental groups for $Al/AlO_X/Al$ junctions (black dots, the references are given in square brackets) are also plotted, the parameters of these samples are listed in Table 2. All the data have been obtained at the base $T < 50$ mK, though the physical temperature of the Josephson circuits has not been directly measured. The Josephson energy $E_J(B)$ for sample 5 was calculated using Equation (2).

Figures 5 and 6 show that the findings are in good agreement with the literature data on the highest values of I_{SW} and lowest values of R_0 measured for low-E_J junctions. Despite large scattering of the data in Figures 5 and 6, a very rapid drop of I_{SW} and increase of R_0 has been observed in most of the experiments as soon as E_J becomes significantly less than 1 K. Figure 5 shows that for typical experimental conditions, the crossover between the "classical" behavior $I_C \propto E_J$ to the behavior controlled by the phase diffusion occurs at $E_J \approx 1$ K. Note that the literature data in Figures 5 and 6 correspond to samples with different values of the ratio E_J/E_C. Given strong scattering of I_{SW} and R_0 , the effect of QPS is hard to detect. For the same reason, it is unclear if the impedance of the environment plays any significant role in these experiments; similar values of I_{SW} could be observed for single JJ in a highly-resistive environment (> 100 kΩ as in [36] and the setup in this work), single JJ in a low-impedance environment [37], and chains of SQUIDs frustrated by the magnetic field [31,35].

The observations are in line with an expected strong dependence of the IPS rate on the sample parameters in the regime $E_C \ll T \leq E_J \ll \Delta$. At $E_J \gg T$, one can estimate the rate of the thermally-generated IPS as $\Gamma = \omega_p exp(-2E_J/k_BT)$, where ω_p is the plasma frequency (or an attempt rate) and $exp(-2E_J/k_BT)$ is the probability of the over-the-barrier excitation. For example, at $E_J = 0.25$ K and $\omega_p/2\pi = 1.32$ GHz, the rate decreases from 3×10^5 s^{-1} to 0.1 s^{-1} if the physical temperature decreases from 50 mK to 20 mK. This might also explain why the experimental results are so sensitive to the noise level in the experimental setup.

Table 2. The literature data on I_{SW} and R_0, ranked by E_J.

Reference	E_J (K)	E_J/E_C	I_C^{AB} (nA)	I_{SW} (nA)	R_0 (kΩ)
Watanabe 2003 [10] sample C	5.7	8	240	40	0.6
Kivioja 2005 [30]	5.2	500	220	145	
Schmidlin 2013 [33], Figure 5.2	2.5	50	106	25	0.13
Shimada 2016 [29], SQUID at $\Phi/\Phi_0 = 0.375$	1.1	14	47	1.2	0.11
Weissl 2015 [36], SQUID at $\Phi/\Phi_0 = 0.26$	0.95	10	38	0.35	0.14
Watanabe 2003 [10] sample G	0.76	1	32		14
Jäck 2015 [38] Figure 4.6	0.54			1.5	13
Senkpiel 2020 [37]	0.47			0.3	33
Senkpiel 2020 [37]	0.23			0.07	143
Yeh 2012 [39]	0.18	1.3	6.5	0.35	31
Jäck 2017 [40]	0.17		7..5	0.05	400
Murani 2020 [14]	0.12		5	0.07	
Senkpiel 2020 [37]	0.09			0.012	830
Kuzmin 1991 [41]	0.05	$\ll 1$		0.014	8000

6. Conclusions and Outlook

Phase slips in JJs have been actively studied over the last three decades in different types of Josephson circuits (single JJs, JJ arrays, etc.) over wide ranges of E_J and E_C. In this work, we focus on the incoherent phase slips, which are expected to become the dominant source of dissipation at sufficiently low temperatures $T \ll \Delta$, where the concentration of quasiparticles becomes negligibly low.

It is observed that in all studied devices with $E_J < 1$ K, the switching current I_{SW} is significantly suppressed with respect to I_C^{AB}. At the same time, a very rapid growth of R_0 with decreasing Josephson coupling below $E_J \approx 1$ K is observed. Large scattering of the data might reflect a steep dependence of the rate of incoherent phase slips on the physical temperature and non-equilibrium noise in different experimental setups. Our observations are consistent with similar data that have been previously reported in the literature.

The observed enhanced dissipation in Josephson circuits with $E_J < 1$ K might impose limitations on the further progress of superconducting qubits based on low-E_J junctions. This important issue requires further theoretical and experimental studies. An especially important direction would be measurements of the coherence time in the qubits with systematically varied Josephson energy over the range E_J = 0.1–1 K. One of the signatures of IPS-induced decoherence might be an observation of a steep temperature dependence of the coherence time at $T < 100$ mK [42].

Author Contributions: Conceptualization, M.E.G. and W.-S.L.; methodology, W.-S.L.; analysis, K.K. and W.-S.L.; design and fabrication, W.-S.L. and P.K.; data curation, W.-S.L.; writing, reviewing and editing, W.-S.L., K.K. and M.E.G.; visualization, T.J.D.; funding acquisition, M.E.G. All authors have read and agreed to the published version of the manuscript.

Funding: The work at Rutgers University was supported by the NSF awards DMR-1708954, DMR-1838979, and the ARO award W911NF-17-C-0024.

Institutional Review Board Statement: Not applicable.

Informed Consent Statement: Not applicable.

Data Availability Statement: Not applicable.

Acknowledgments: The authors would like to thank Srivatsan Chakram for insightful discussions.

Conflicts of Interest: The authors declare no conflicts of interest.

Abbreviations

The following abbreviations are used in this manuscript:

JJs	Josephson Junctions
IPS	Incoherent Phase Slips
QPS	Quantum Phase Slip
IVC	Current-Voltage Characteristics
IZ	Ivanchenko and Zilberman
SQUIDs	Superconducting Quantum Interference Devices

Appendix A. Device Design and Fabrication

The Josephson junctions in this work were fabricated by the Manhattan pattern technique with multi-angle deposition of Al electrodes through a bilayer e-beam resist mask [43]. The oxidation process performed between depositions of the bottom and top aluminum electrodes has been optimized for fabrication of junctions with required values of E_J and minimal scattering of junction parameters. Typically, the dry oxygen partial pressure $1-100$ torr and oxidized the structures for 5–15 min were used. The standard deviation of the normal state resistance R_N across the 7 mm$\times$ 7 mm chip did not exceed 10% for sub-μm-wide junctions with $R_N \sim 1$ kΩ and 30% for the junctions with $R_N \sim 100$ kΩ. The junction area variations did not exceed 10% across a 200 μm-long chain.

All the samples studied in this work have been implemented as SQUIDs, in order to be able to in-situ tune E_J by applying the external magnetic field. Figure A1 schematically shows the design of a chain of SQUIDs formed by small junctions (0.2×0.2 μm^2). The area of the SQUID loop varied between 6 μm^2 and 49 μm^2. In this work, the experiments are focused on the JJs with 1 K $> E_J \gg E_C$; this regime is relevant to the quantum circuits in which JJs are shunted with large external capacitors (such as the transmon qubit). Large E_J/E_C ratio also significantly reduces the rate of quantum phase slips $\Gamma_{QPS} \propto exp(-2\sqrt{E_J/E_C})$ [13]. The specific capacitance of the tunneling AlO_X barrier is about 50 fF/μm^2, and in order to reduce E_C down to $\sim$10 mK, the junctions should either have relatively large in-plane dimensions ($A_{JJ} > 4$ μm^2) or be shunted with external capacitors ($C_g > 200$ fF). Both methods are used in different structures. In the approach where relatively large JJs are introduced in order to keep E_J below 1 K, the oxidation recipes are fine-tuned for the growth of low-transparency tunneling AlO_X barrier. In the "external capacitor" approach, several designs of the shunting capacitors have been implemented. Figure A1 shows that each SQUID unit cell is flanked by two large metal pads, which are used as shunting capacitors C_g to the common ground when the entire chain was covered by an additional top electrode (sputtered Pt film). A few nm thick native AlO_X oxide grown at the atmospheric pressure serves as a pinhole-free dielectric for this parallel-plate C_g with a typical capacitance around 500 fF for 50 μm^2 pad area. Such C_g corresponds to a charging energy per each cell as low as $E_C = (2e)^2/2C = 8$ mK.

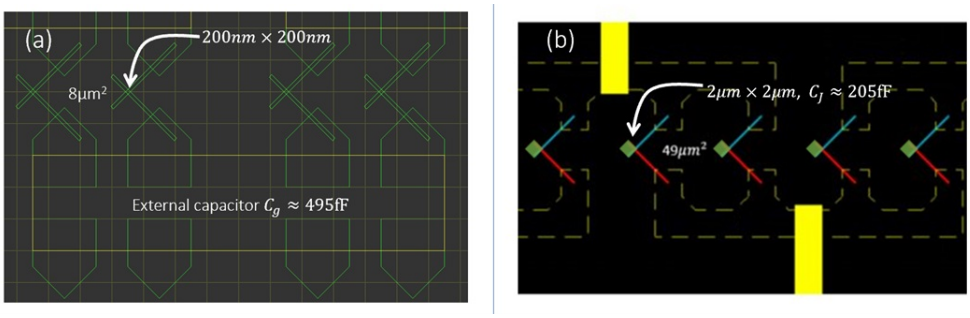

Figure A1. Various designs of SQUIDs. (**a**) Each SQUID unit cell was shunted by a large $\mathbf{C_g \approx 0.5pF}$ the ground. The common ground electrode is shown by a yellow rectangle. (**b**) SQUIDs formed by large JJs with junction area $\mathbf{A_{JJ} \approx 2.2\ ^{-}m^2}$. Yellow rectangles show electrodes used to measure the IVC of individual SQUIDs.

Appendix B. Measurement Setup

To measure the IVC of low-E_J junctions with small switching currents (typically, within the pA-nA range), careful filtering of noise in the measurement circuit is required (see, e.g., [25]). Our measurement setup included the cascaded low pass filters shown in Figure A2. The wiring for DC setup inside the cryostat consists of 12 twisted pairs made of resistive alloys $CuNi$:$NbTi$ (5:1) with multiple thermal anchoring points. Near the cold finger which supported the sample holder, about 1-meter-long twisted pairs are used as central conductors of the copper-powder-epoxy lowpass filter with the cut-off frequency ∼100 MHz (see, e.g., [44]); this filter also provides thermal anchoring of all wires before connecting to the sample. On the sample holder, 100 kΩ surface mount metal-film resistors with low parasitic capacitance have been installed in each lead. The voltage across the sample was amplified by a preamplifier (DL Instrument 1201) with a few GΩ input impedance.

The circuit outside of the dilution refrigerator (Figure A2) included a commercial LC low pass filter (BLP 1.9+, DC−1.9 MHz) and a homemade RC filter (DC−8Hz) box with variable biasing resistors up to 1 GΩ. The voltage drop across the sample was amplified with a voltage preamp DL1201 and measured by HP 34401A digital multimeter.

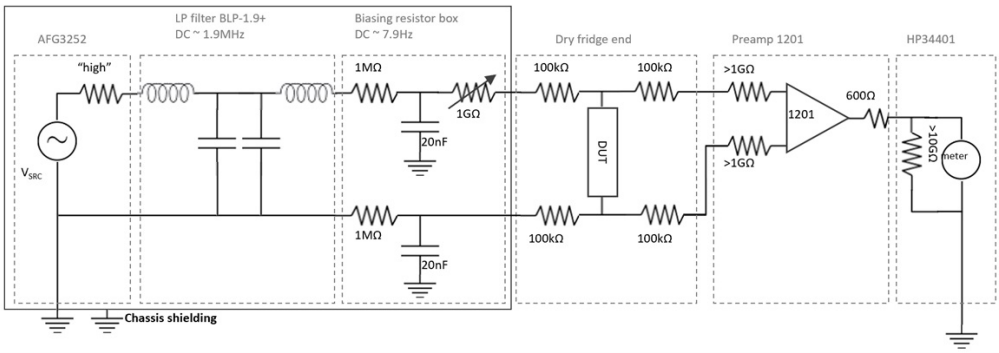

Figure A2. The wiring schematics for DC current source measurements. The device-under-test (DUT) was mounted inside a sample holder thermally anchored to the mixing chamber of the dilution refrigerator.

Appendix C. The Effect of Noise on the Current-Voltage Characteristics

In this work, the noise reduction is the primary concern in characterization of low-E_J junctions, and most of the measurements have been performed in the constant current mode. According to Equation (1), $I_C^{AB} = 30$ nA at $T = 0$ for an $Al/AlOx/Al$ JJ with $E_J = 1$ K. With further reduction of E_J and increase of the phase slip rate, the current range well below 1 nA becomes relevant.

Figure A3 illustrates the importance of proper filtering of noises in both the current supply part and the voltage recording part of the measuring setup. By using the combi-

nation of cascaded low-pass filters and 100 kΩ resistors on the sample holder, switching currents in the pA range precision are achieved (Figure 2c of the main text).

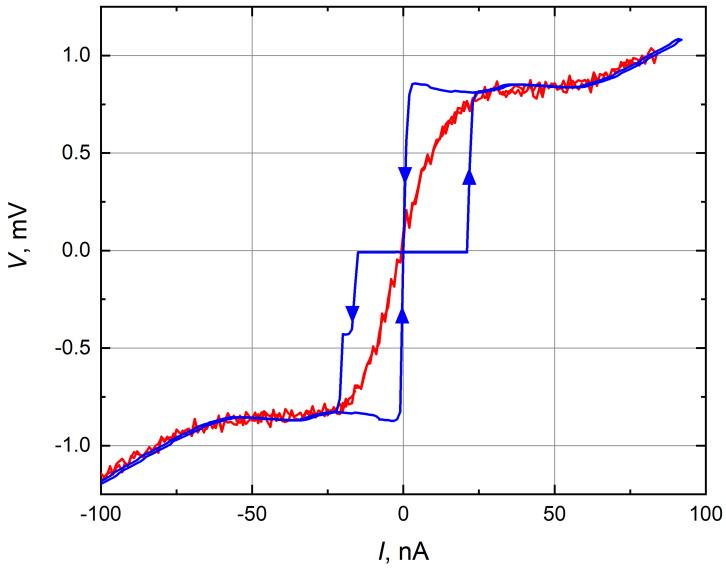

Figure A3. The IVC recorded for a two-unit SQUID device with different measurement setups at $T = 25$ mK (sample 3 in Table 1). Without thorough filtering, the IVC was non-hysteretic and smeared. Proper filtering of all leads enables observation of a well-developed hysteresis expected for an underdamped junction at low T.

Appendix D. Modeling the Effect of Thermal Noise

The theory of the DC transport in underdamped Josephson junctions in presence of a stochastic noises has been developed by Ivanchenko and Zilberman [28]. According to the Ivanchenko–Zilberman (IZ) model, a voltage-biased Josephson junction is subject to thermal noise of the biasing resistor which causes phase diffusion (see Equation (4) in the main text). By solving the corresponding Fokker–Planck equation, the superconducting part of the current as a function of bias voltage V_B can be found as:

$$I_S = I_C \times Im[\frac{J_{1-i\alpha\nu}(\alpha)}{J_{i\alpha\nu}(\alpha)}], \tag{A1}$$

where $\alpha = \frac{E_J}{k_B T}$, $\nu = \frac{V_B}{I_C R}$ and J_{a+ib} is the modified Bessel function. In the limit of a small Josephson energy $E_J \ll k_B$, this expression is simplified:

$$I_S = \frac{I_C R}{2} \frac{V_B}{V_B^2 + V_n^2} \tag{A2}$$

$$V_n = \frac{2e}{\hbar} R k_B T \tag{A3}$$

The maximum current that can be carried by Cooper pairs is realized at $V_B = V_n$ (V_n is the Johnson noise from the resistor R); the further increase of the biasing current leads to switch to the resistive state. As Figure A4b shows, the value of the switching current predicted by the classical IZ (cIZ) model starts to deviate from I_C^{AB} for the junction with $E_J < 1$ K. The maximum value of the switching current is realized at a non-zero voltage V_n, which depends only on the voltage noise amplitude, so the zero-bias resistance in the IPS regime is expected to scale as E_J^{-2}.

In the case when a system is subject to other sources of noise such as the thermal noise across the junction capacitance or the external electromagnetic noise due to insufficient

filtering, the modified IVC can be calculated by convolving the cIZ curve with Gaussian-distributed V_B of the width corresponding to the noise amplitude V_{noise} (Figure A4a,b). As Figure A4b shows, the cIZ model can explain qualitatively the switching current behavior in systems with low Josephson energy, the value of the excessive noise V_{noise} could be used as a fitting parameter to obtain quantitative agreement.

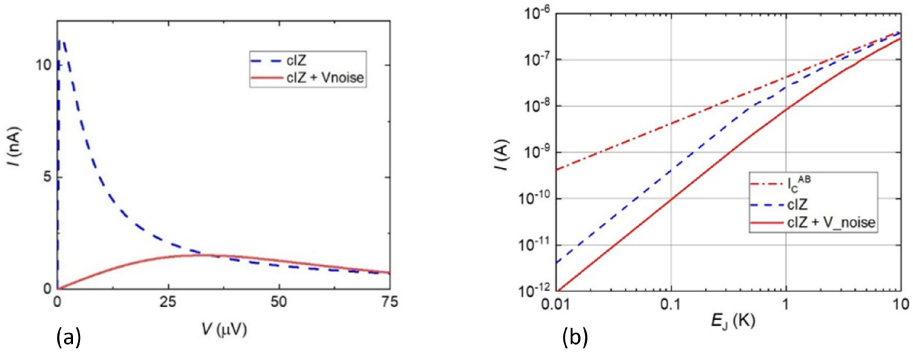

Figure A4. (**a**) The supercurrent branch of the IVC of a JJ with $E_J = 1$ K at $T = 50$ mK, predicted by the classical IZ theory (dashed line) and its modification in presence of gaussian noise with amplitude 24 μV (solid line). (**b**) Nominal critical current (dot-dashed line), switching current according to the IZ theory without (dashed line) and with (solid line) extra voltage noise of the same amplitude.

References

1. Nguyen, L.B.; Lin, Y.-H.; Somoroff, A.; Mencia, R.; Grabon, N.; Manucharyan, V.E. High-Coherence fluxonium qubit. *Phys. Rev. X* **2019**, *9*, 041041. [CrossRef]
2. Gyenis, A.; Mundada, P.S.; Paolo, A.D.; Hazard, T.M.; You, X.; Schuster, D.I.; Koch, J.; Blais, A.; Houck, A.A. Experimental realization of a protected superconducting circuit derived from the 0–π qubit. *PRX Quantum* **2021**, *2*, 010339. [CrossRef]
3. Zhang, H.; Chakram, S.; Roy, T.; Earnest, N.; Lu, Y.; Huang, Z.; Weiss, D.K.; Koch, J.; Schuster, D.I. Universal fast-flux control of 387 a coherent, low-frequency qubit. *Phys. Rev. X* **2021**, *11*, 011010.
4. Peruzzo, M.; Trioni, A.; Hassani, F.; Zemlicka, M.; Fink, J.M. Surpassing the resistance quantum with a geometric superinductor. *Phys. Rev. Appl.* **2020**, *14*, 044055. [CrossRef]
5. Somoroff, A.; Ficheux, Q.; Mencia, R.A.; Xiong, H.; Kuzmin, R.V.; Manucharyan, V.E. Millisecond coherence in a superconducting qubit. *arXiv* **2021**, arXiv:2103.08.
6. Tinkham, M. *Introduction to Superconductivity*; Dover Publications: Mineola, NY, USA, 1996
7. Martinis, J.M.; Kautz, R.L. Classical phase diffusion in small hysteretic Josephson junctions. *Phys. Rev. Lett.* **1989**, *63*, 1507–1510. [CrossRef]
8. Kautz, R.L.; Martinis, J.M. Noise-affected i-v curves in small hysteretic Josephson junctions. *Phys. Rev. B* **1990**, *42*, 9903. [CrossRef]
9. Eiles, T.M.; Martinis, J.M. Combined Josephson and charging behavior of the supercurrent in the superconducting singleelectron transistor. *Phys. Rev. B* **1994**, *50*, 627–630. [CrossRef]
10. Watanabe, M.; Haviland, D.B. Quantum effects in small-capacitance single Josephson junctions. *Phys. Rev. B* **2003**, *67*, 094505. [CrossRef]
11. Fazio, R.; van der Zan, H. Quantum phase transitions and vortex dynamics in superconducting networks. *Phys. Rep.* **2001**, *355*, 235–334. [CrossRef]
12. Bard, M.; Protopopov, I.V.; Gornyi, I.V.; Shnirman, A.; Mirlin, A.D. Superconductor-insulator transition in disordered Josephson-junction chains. *Phys. Rev. B* **2017**, *96*, 064514. [CrossRef]
13. Ast, C.R.; Jäck, B.; Senkpiel, J.; Eltschka, M.; Etzkorn, M.; Ankerhold, J.; Kern, K. Sensing the quantum limit in scanning tunnelling spectroscopy. *Nat. Commun.* **2016**, *7*, 13009. [CrossRef] [PubMed]
14. Murani, A.; Bourlet, N.; Sueur, H.; Portier, F.; Altimiras, C.; Esteve, D.; Grabert, H.; Stockburger, J.; Ankerhold, J.; Joyez, P. Absence of a dissipative quantum phase transition in Josephson junctions. *Phys. Rev. X* **2020**, *10*, 021003. [CrossRef]
15. Matveev, K.A.; Larkin, A.I.; Glazman, L.I. Persistent Current in Superconducting Nanorings. *Phys. Rev. Lett.* **2002**, *89*, 096802. [CrossRef]
16. Manucharyan, V.E.; Masluk, N.A.; Kamal, A.; Koch, J.; Glazman, L.I.; Devoret, M.H. Evidence for coherent quantum phase slips across a Josephson junction array. *Phys. Rev. B* **2012**, *85*, 024521. [CrossRef]
17. Koch, J.; Yu, T.M.; Gambetta, J.; Houck, A.A.; Schuster, D.I.; Majer, J.; Blais, A.; Devoret, M.H.; Girvin, S.M.; Schoelkopf, R.J. Charge-insensitive qubit design derived from the Cooper pair box. *Phys. Rev. A* **2007**, *76*, 042319. [CrossRef]

18. Gyenis, A.; Paolo, A.D.; Koch, J.; Blais, A.; Houck, A.A.; Schuster, D.I. Moving beyond the transmon: Noise-Protected superconducting quantum circuits. *PRX Quantum* **2021**, *2*, 030101. [CrossRef]
19. NEarnest; Chakram, S.; Lu, Y.; Irons, N.; Naik, R.K.; Leung, N.; Ocola, L.; Czaplewski, D.A.; Baker, B.; Lawrence, J.; Koch, J.; Schuster, D.I. Realization of a Λ system with metastable states of a capacitively shunted fluxonium. *Phys. Rev. Lett.* **2018**, *120*, 150504. [CrossRef]
20. Mooij, J.E.; Nazarov, Y.V. Superconducting nanowires as quantum phase-slip junctions. *Nat. Phys.* **2006**, *2*, 169–172. [CrossRef]
21. Astafiev, O.V.; Ioffe, L.B.; Kafanov, S.; Pashkin, Y.A.; Arutyunov, K.Y.; Shahar, D.; Cohen, O.; Tsai, J.S. Coherent quantum phase slip. *Nature* **2012**, *484*, 355. [CrossRef]
22. Svetogorov, A.E.; Taguchi, M.; Tokura, Y.; Basko, D.M.; Hekking, F.W.J. Theory of coherent quantum phase slips in Josephson junction chains with periodic spatial modulations. *Phys. Rev. B* **2018**, *97*, 104514. [CrossRef]
23. Arutyunov, K.Y.; Golubev, D.S.; Zaikin, A.D. Superconductivity in one dimension. *Phys. Rep.* **2008**, *464*, 1–70. [CrossRef]
24. Semenov, A.G.; Zaikin, A.D. Quantum phase slip noise. *Phys. Rev. B* **2016**, *94*, 014512. [CrossRef]
25. Schön, G.; Zaikin, A.D. Quantum coherent effects, phase transitions, and the dissipative dynamics of ultra small tunnel junctions. *Phys. Rep.* **1990**, *198*, 237–412. [CrossRef]
26. Vion, D.; Götz, M.; Joyez, P.; Esteve, D.; Devoret, M.H. Thermal activation above a dissipation barrier: Switching of a small Josephson junction. *Phys. Rev. Lett.* **1996**, *77*, 3435–3438. [CrossRef] [PubMed]
27. Fistul, M.V. Josephson phase diffusion in small josephson junctions: A strongly nonlinear regime. In *No-Nonsense Physicist*; Polini M., Vignale G., Pellegrini V., Jain J.K., Eds.; Publications of the Scuola Normale Superiore; Edizioni della Normale: Pisa, Italy, 2016; Volume 2, pp. 73–80.
28. Ivanchenko, Y.M.; Zil'berman, L.A. The Josephson effect in small tunnel contacts. *Sov. Phys. JETP* **1969**, *28*, 1272.
29. Shimada, H.; Katori, S.; Gandrothula, S.; Deguchi, T.; Mizugaki, Y. Bloch oscillation in a one-dimensional array of small Josephson junctions. *J. Phys. Soc. Jpn.* **2016**, *85*, 074706. [CrossRef]
30. Kivioja, J.M.; Nieminen, T.E.; Claudon, J.; Buisson, O.; Hekking, F.W.J.; Pekola, J.P. Observation of transition from escape dynamics to underdamped phase diffusion in a Josephson junction. *Phys. Rev. Lett.* **2005**, *94*, 247002. [CrossRef]
31. Lu, W.-S. Josephson Circuits for Protected Quantum Bits. Ph.D. Thesis, Rutgers University, New Brunswick, NJ, USA, 2021.
32. McCumber, D.E. Effect of ac impedance on dc Voltage-Current characteristics of superconductor Weak-Link junctions. *J. Appl. Phys.* **1968**, *39*, 3113–3118. [CrossRef]
33. Schmidlin, S. Physics and Technology of small Josephson junctions. Ph.D. Thesis, Royal Holloway, University of London, Egham, UK, 2013.
34. Coon, D.D.; Fiske, M.D. Josephson ac and step structure in the supercurrent tunneling characteristic. *Phys. Rev.* **1965**, *138*, A744–A746. [CrossRef]
35. Wilen, C.D.; Abdullah, S.; Kurinsky, N.A.; Stanford, C.; Cardani, L.; D'Imperio, G.; Tomei, C.; Faoro, L.; Ioffe, L.B.; Liu, C.H.; et al. Correlated charge noise and relaxation errors in superconducting qubits. *Nature* **2021**, *594*, 369–373. [CrossRef] [PubMed]
36. Weißl, T.; Rastelli, G.; Matei, I.; Pop, I.M.; Buisson, O.; Hekking, F.W.J.; Guichard, W. Bloch band dynamics of a Josephson junction in an inductive environment. *Phys. Rev. B* **2015**, *91*, 014507. [CrossRef]
37. Senkpiel, J.; Dambach, S.; Etzkorn, M.; Drost, R.; Padurariu, C.; Kubala, B.; Belzig, W.; Yeyati, A.L.; Cuevas, J.C.; Ankerhold, J.; Ast, C.R.; Kern, K. Single channel Josephson effect in a high transmission atomic contact. *Commun. Phys.* **2020**, *3*, 1–6. [CrossRef]
38. Jäck, B. Josephson Tunneling at the Atomic Scale. Ph.D. Thesis, EPFL, Lausanne, Switzerland, 2015.
39. Yeh, S.-S.; Chen, K.-W.; Chung, T.-H.; Wu, D.-Y.; Lin, M.-C.; Wang, J.-Y.; Ho, I.-L.; Wu, C.-S.; Kuo, W.; Chen, C. A method for determining the specific capacitance value of mesoscopic Josephson junctions. *Appl. Phys. Lett.* **2012**, *101*, 232602. [CrossRef]
40. Jäck, B.; Senkpiel, J.; Etzkorn, M.; Ankerhold, J.; Ast, C.R.; Kern, K. Quantum brownian motion at strong dissipation probed by superconducting tunnel junctions. *Phys. Rev. Lett.* **2017**, *119*, 147702. [CrossRef]
41. Kuzmin, L.S.; Nazarov, Y.V.; Haviland, D.B.; Delsing, P.; Claeson, T. Coulomb blockade and incoherent tunneling of cooper pairs in ultrasmall junctions affected by strong quantum fluctuations. *Phys. Rev. Lett.* **1991**, *67*, 1161–1164. [CrossRef] [PubMed]
42. Manucharyan, V. Private Communication, 2020.
43. Bell, M.T.; Sadovskyy, I.A.; Ioffe, L.B.; Kitaev, A.Y.; Gershenson, M.E. Quantum superinductor with tunable nonlinearity. *Phys. Rev. Lett.* **2012**, *109*, 137003. [CrossRef]
44. Martinis, J.M.; Devoret, M.H.; Clarke, J. Experimental tests for the quantum behavior of a macroscopic degree of freedom: The phase difference across a Josephson junction. *Phys. Rev. B* **1987**, *35*, 4682–4698 . [CrossRef]